Office Note Series on Global Modeling and Data Assimilation

Tangent Linear Analysis of the Mosaic Land Surface Model

Runhua Yang*, Stephen E. Cohn, Arlindo da Silva, Joanna Joiner, Paul R. Houser

Data Assimilation Office, Goddard Laboratory for Atmospheres
*Science Systems and Applications Inc., Data Assimilation Office

Abstract

In this study, a tangent linear eigenanalysis is applied to the Mosaic land surface model (LSM) (Koster and Suarez 1992) to examine the impacts of the model internal dynamics and physics on the land surface state variability. The tangent linear model (TLM) of the Mosaic LSM is derived numerically for two sets of basic states and two tile types of land condition, grass and bare soil. An additional TLM, for the soil moisture subsystem of this LSM, is derived analytically for the same cases to obtain explicit expressions for the eigenvalues. An eigenvalue of the TLM determines a characteristic time scale, and the corresponding eigenvector, or mode, describes a particular coupling among the perturbed states. The results show that (1) errors in initial conditions tend to decay with e-folding times given by the characteristic time scales; (2) the LSM exhibits a wide range of internal variability, modes mainly representing surface temperature and surface moisture perturbations exhibit short time scales, whereas modes mainly representing deep soil temperature perturbations and moisture transfer throughout the entire soil column exhibit much longer time scales; (3) the modes of soil moisture tend to be weakly coupled with other perturbed variables, and the mode representing the deep soil temperature perturbation has a consistent e-folding time across the experiments; (4) the key parameters include soil moisture, soil layer depth, soil hydraulic parameters, and soil moisture transfer process.

The results qualitatively agree with previous findings. However, tangent linear eigenanalysis provides a new approach to the quantitative substantiation of those findings. Also, it reveals the evolution and the coupling of the perturbed land states that are useful for the development of land surface data assimilation schemes. We must be careful when generalizing the quantitative results since they are obtained with respect to two specific basic states and two simple land conditions. Also, the methodology employed here does not apply directly to an actual time-varying basic state.

Contents

List of Figures

List of Tables

1   Introduction

A land surface model (LSM) or soil-vegetation-atmosphere-transfer (SVAT) scheme exhibits variability on a wide range of time scales from hours to months, and even years through atmospheric interactions (i.e., Delworth and Manabe 1988, 1993; Entekhabi 1995; Robock et al. 1998). These time scales are strongly determined by external forcing, especially precipitation and downward short-wave and long-wave radiation at the surface. They are also modulated by the internal dynamics and physics of land surface systems, in particular by soil moisture dynamics. There are numerous studies on the variability of land surface models. Approaches to date include: 1) performing numerical simulations, 2) performing numerical sensitivity tests, and 3) building relatively simple land surface models that can be solved analytically.

In the first approach, either a general circulation model (GCM) which includes an LSM or a stand-alone LSM is integrated over long time periods (i.e., Dickinson et al. 1984; Sato et al. 1989; Koster and Suarez, 1994). These studies have demonstrated the main variability of the land surface system, as modeled, and the pronounced effect of the land surface on atmospheric variability. In the second approach, using either an LSM coupled to a GCM or a stand-alone LSM, sensitivity experiments are usually performed with a change in one particular parameter or parameterization scheme (e.g., Henderson-Sellers et al. 1995; Xue et al. 1996a, 1996b). The results are then compared with a control integration to reveal the impact of the change. This type of sensitivity experiment identifies important parameters or parameterizations in land surface models. The third approach, solving equations of a simple LSM analytically, estimates characteristic time scales of land surface variables in simplified cases (e.g., Delworth and Manabe 1988; Brubaker and Entekhabi 1995; Yang et al. 1995). This approach simplifies complex land surface processes. For example, one can represent the evaporation and runoff process as a bucket model or treat the soil moisture system as a first-order Markov process.

These three approaches mainly reveal the impact of external forcing (Entekhabi 1995; Delworth and Manabe 1988, 1993) on the land surface variability, because the forcing terms exert the dominant control on the variability of land surface models. In the data assimilation context, we need to understand the impact of internal dynamics and physics on the variability of a land surface model. For this purpose we employ tangent linear analysis to an LSM in this study.

There are two reasons for studying the internal dynamics and physics of land surface models with the tangent linear approximation. First, the linear behavior of the internal dynamics and physics alone controls the land surface state perturbations, which are defined as the departures from a solution of a nonlinear model called the trajectory. These perturbations might be considered to be errors from true state values. The study of this linear behavior allows us to identify the main relationships among these errors in an LSM, called the balance. An example of such a balance is the effect of errors in surface soil moisture on the surface temperature and moisture. This kind of error correlation may be used as background error covariances of an assimilation scheme. Second, with an understanding of the internal features, we can efficiently identify key parameters and parameterizations of the model with minimum influence of the external forcing. By efficiently we mean that one run can reveal multiple key parameters or parameterizations. By minimum influence of the external forcing we mean that the evolution of the perturbed state variables is no longer explicitly controlled by the external forcing, though the mean trajectory is controlled by the external forcing and the perturbation behavior may vary with different mean states.

In this paper, we apply tangent linear model (TLM) analysis to study the linear behavior of the internal physics and dynamics of the Mosaic LSM (Koster and Suarez 1992). In a recent review paper, Errico (1997) describes the development and applications of TLM and their corresponding adjoint models in meteorology. Although the use of TLM and adjoint models

has recently increased rapidly, its applications to land surface modeling and assimilation require specific consideration due to the complex physical features and non-linearity of LSMs.

In Section 2, we briefly describe the Mosaic LSM. In Section 3, we derive the TLM based on the prognostic equations of the Mosaic LSM, and we describe the experimental design and precautions taken in deriving the TLM numerically. In Section 4, we present the results of the TLM eigenanalysis, including characteristic time scales and modes of the land surface state perturbations. In Section 5, we obtain a linearized soil moisture subsystem and examine the role of soil moisture dynamics. We find explicit relationships between the time scales and the Mosaic LSM parameters. Finally, in Section 6, we summarize the main results and discuss their application to land surface data assimilation.

2   Description of Mosaic land surface model

The Mosaic LSM (Koster and Suarez 1992) is named for its use of a "mosaic" strategy to account for subgrid heterogeneity in surface characteristics. In the Mosaic LSM, every grid cell is subdivided into homogeneous subregions, or "mosaic tiles". Each tile contains a single vegetation or bare soil type. Energy and water balance calculations are performed over each tile. The tiles in a grid cell respond to the grid-cell mean conditions in the overlying atmosphere. This grid cell, in turn, responds to the area-weighted fluxes of heat and moisture from the tiles (Koster and Suarez 1996).

The Mosaic LSM is based on the Simple Biosphere (SiB) model of Sellers et al. (1986), and includes complex biophysical processes. Similarly to SiB, it calculates the energy and water transfers using an electrical resistance network analog. For example, to calculate the latent heat flux (current) along a given pathway, the difference between surface and atmospheric vapor pressures (potentials) is divided by an effective resistance, which is a function of the atmospheric conditions and of plant and soil properties. Similarly, the sensible heat flux is determined by the difference between the temperatures (potentials) of the surface and the atmosphere. Koster and Suarez (1994) have conducted a 20-year long simulation with a GCM coupled with Mosaic LSM, and concluded that the simulation of hydrology cycle is improved using Mosaic LSM. The Mosaic LSM has also been successfully implemented in the Goddard Earth Observing System General Circulation Model of the Data Assimilation Office, Goddard Space Flight Center of NASA (Molod, 1999).

The eight prognostic variables in each tile of the Mosaic LSM are:

T_c: temperature of the surface/canopy system

T_d: temperature in deep soil

W_c: moisture in the canopy interception reservoir

W_i (i=1,2,3): moisture in the top, middle, and bottom soil layers, respectively

S: water equivalent in the snowpack, if any

e_a: vapor pressure in the near-surface layer (within the canopy for the vegetation tiles).

The prognostic equations are as follows:

$$C_H \frac{dT_c}{dt} = R_{sw-net} + R_{lw}^{\downarrow} - R_{lw}^{\uparrow} - H - \lambda E - G_d, \tag{1}$$

$$C_{H-deep}\frac{dT_d}{dt} = G_d, \tag{2}$$

$$\frac{dW_c}{dt} = P + S_{melt} - E_{int} - P_T, \tag{3}$$

$$\frac{dW_1}{dt} = P_T - R_s - E_{bs} - E_{transp,1} - Q_{1,2}, \tag{4}$$

$$\frac{dW_2}{dt} = Q_{1,2} - E_{transp,2} - Q_{2,3}, \tag{5}$$

$$\frac{dW_3}{dt} = Q_{2,3} - Q_{3,\infty}, \tag{6}$$

$$\frac{dS}{dt} = P_s - S_{melt} - E_{snow}. \tag{7}$$

The prognostic equation for surface layer or canopy air vapor pressure (e_a) is

$$\frac{dE}{dt} = \frac{\partial E}{\partial T_c}\frac{dT_c}{dt} + \frac{\partial E}{\partial e_a}\frac{de_a}{dt}, \tag{8}$$

where

$$E = \frac{\rho \epsilon}{p_s}[\frac{e_s(T_c) - e_a}{r_{eff}(T_c, e_a)}].$$

The terms in the equations are:

C_H: heat capacity of surface or canopy system

R_{sw-net}: net short-wave radiation at surface

$R_{lw}^{\downarrow}$: downward long-wave radiation at surface

$R_{lw}^{\uparrow}$: upward long-wave radiation at surface

H: sensible heat flux

λE: latent heat flux

G_d: heat flux to deep soil

C_{H-deep}: heat capacity of deep soil

P: rainfall rate

S_{melt}: snow-melt rate

E_{int}: evaporation of intercepted water

P_T: throughfall rate of precipitation

R_s: surface runoff rate

E_{bs}: evaporation rate from bare surface

$E_{transp,i}$ (i=1,2): water removal rate via transpiration from the ith soil layer

$Q_{i,j}$: moisture flux from i^{th} soil layer to j^{th} soil layer

P_s: snowfall rate

E_{snow}: snow sublimation rate

e_s: saturation vapor pressure, a function of T_c

r_{eff}: effective surface resistance to vapor transport, a function of T_c and e_a

ρ: air density

ϵ: ratio of the molecular weight of water vapor to that of dry air

p_s: surface pressure.

The details of the derivation are given in Koster and Suarez (1992, 1994, 1996).

3   TLM derivation and experimental design

3.1   Tangent linear model derivation

Let X denote the vector of prognostic (state) variables. Written as a system of eight ordinary differential equations, the general form of equations (1)-(8) is

$$\frac{dX}{dt} = F(X) + \text{external forcing}, \tag{9}$$

where the vector $F(X)$ can be represented by $F(X) = (F_1, F_2, ..., F_8)^T$ denoting the internal dynamics and physical processes such as soil moisture dynamics, and the superscript T denotes the transpose. External forcing terms are the near-surface atmospheric conditions, including precipitation and downward solar and longwave radiation fluxes at the surface. These terms do not depend explicitly on the land surface state X.

A perturbation method is used to linearize the nonlinear system (9). A solution X of equation (9) is decomposed into a *"basic state"* $\bar{X} = \bar{X}(t)$ satisfying (9), plus a perturbation X':

$$X = \bar{X} + X'. \tag{10}$$

The Taylor expansion of F around the basic state $\bar{X}$ is

$$F_i(X) = F_i(\bar{X}) + \sum_j \left(\frac{\partial F_i}{\partial X_j} \bigg|_{X_j = \bar{X}_j} \right) X'_j + O(X'^2). \tag{11}$$

Substituting equations (10) and (11) into the system (9) and neglecting the higher-order terms, we obtain the tangent linear model:

$$\frac{dX'}{dt} = AX', \tag{12}$$

4

where $A_{ij} \equiv \left(\frac{\partial F_i}{\partial X_j} \Big|_{X_j = \bar{X}_j} \right)$, and $A = A(\bar{X}(t))$ is the tangent linear matrix or Jacobian, representing the sensitivity of the functions to infinitesimal change in X. The basic state $\bar{X}$ denotes a solution of the nonlinear system (9), called the model trajectory in a data assimilation context, and can be chosen as a statistical average of states. The linear system (12) approximates the evolution of an initial error $X'(0) \equiv X'(t = 0)$ in that trajectory. Since the linear system (12) eliminates the external forcing term, the behavior of $X'(t)$ is determined primarily by the internal physics and dynamics of the Mosaic LSM in the vicinity of the basic state. Dependence of $X'(t)$ on the external forcing is implicit, through the dependence of $A(\bar{X}(t))$ on the basic state.

We study the behavior of (12) for A evaluated either at a specific time or for a specific time-mean state. This simplifies the problem considerably, for in each case A is then independent of time. The solution of (12) is then just

$$X'(t) = e^{At} X'(0).$$ (13)

The eigendecomposition of A is given by

$$A = U \Lambda U^{-1},$$ (14)

where Λ is the diagonal matrix of eigenvalues of A, and the columns of U are the corresponding eigenvectors. An eigenvector (mode) corresponding to a given eigenvalue expresses a specific coupling among the variables $X'(t)$. Note that A is not symmetric and its eigenvectors are not mutually orthogonal.

Since we consider A to be independent of time, the stability of the linear system (12) depends on the eigenvalues Λ. If all eigenvalues have negative real parts, the system is stable for the basic state we consider, and any initial error will decay with time; if any one of the eigenvalues has a positive real part, the system is unstable. If all eigenvalues are real, the solutions are non-oscillatory. A negative eigenvalue λ represents a decay rate with e-folding time $\tau = \frac{-1}{\lambda}$.

3.2 Experimental design

The purpose of the experiments is to use tangent linear analysis as a new method for understanding the internal dynamics and physics of an LSM. As we showed in the previous section, the construction of A depends on the mean state. Therefore, application of the TLM to a site with a specific mean state and land cover condition is similar to a case study. However, we anticipate that this kind of case study reveals some common features of the land-surface state given more general forcing terms and suitable land conditions. This will be shown in the following section.

The site presented in the model is the HAPEX-Mobilhy Caumont site, in France ($43^0 41' N$, $0^0 6' W$). The canopy for that site is prescribed as 90% grass and 10% bare soil. We perform four experiments with a combination of two considerably different sets of vegetation parameters and basic states. We then examine the temporal variation and relationships among the perturbed state variables. In experiments one and two (EXP 1, EXP 2), the vegetation type is grass, with two different basic states. In experiments three and four (EXP 3, EXP 4), the vegetation type is bare soil, and the same basic states of EXP 1 and EXP 2 are used. We describe one vegetation type as grass because that is the real land condition at the HAPEX site. We chose another vegetation type as bare soil for the

contrast, but it is not totally unreasonable since the site is covered by 10% bare soil. To simplify the derivation in section 5, only one type of vegetation is used in each experiment. This simplification neglects the Mosaic "tile" properties of the model.

The basic state is selected from a 3-year long control integration forced each year with a one-year record of near-surface atmospheric conditions at the HAPEX-Mobilhy Caumont site. The purpose of the control run is two-fold. First, it shows the length of time required for the Mosaic LSM to arrive at equilibrium under the chosen conditions. Second, it provides appropriate basic state values for the four experiments. The near-surface atmospheric forcing at the HAPEX site is available at 30-minute time intervals for 1986. When the data were unavailable, neighboring meteorological stations were selected to provide the required information (Goutorbe 1991; Goutorbe and Tarrieu 1991). This data set has been used in the Project for Intercomparison of Land-surface Parameterization schemes Phase 2 (PILPS-2) experiments (Henderson-Sellers et al. 1993). The forcing terms include downward shortwave and longwave radiation, precipitation, air temperature, 2-meter specific humidity, 2-meter wind speed, and surface pressure.

We selected two basic states, the state at 13Z June 1, 1986, and the June monthly mean state at 13Z, from the second year of the control run, since the Mosaic LSM reaches an equilibrium state in about six months. During the second year, surface fluxes and the state variables, is almost the same as that of the first year starting from July, and the output of the third year is overlapped with that of the second year. The other input parameters for the TLM correspond to these two situations. We selected a time close to local noontime and a summer month because the land-surface thermal activity is most active then. Due to the lack of snow cover during this time and interception storage over grass, the original eight prognostic equations are reduced to six. The counterparts of equations (3) and (7) are therefore eliminated from the TLM (equation 12). However, this simplification excludes the variability induced by those two processes. Some previous studies (i.e., Scott et al., 1995; Koster and Suarez, 1994; Schlosser et al. 1997) show the importance of these processes in some regions.

The observational data are very limited at this site. We compared the model results for June with the available observations. The magnitudes of the model sensible heat and latent heat fluxes are comparable with the observations. The model soil moisture content within the top 50 cm column is consistently lower than that observed by neutron sounding probes measuring once every week. Since we do not know the observed soil porosity values, we are not able to calculate the plant-available soil moisture as suggested by Robock et al. (1998). However, the Mosaic LSM has been an active participant in PILPS, which, among other things, tested its ability to reproduce observed surface fluxes in response to observed meteorological forcing. PILPS tests at Cabauw in the Netherlands (Chen et al., 1997) and across the Red-Arkansas river basin in the U.S. (Wood et al., 1998; Liang et al., 1998;) show that the Mosaic model, though not perfect, does produce reasonably realistic evaporation and runoff rates.

Figure 1 shows the monthly-mean diurnal cycle of the land surface variables for June. The canopy air vapor pressure (e_a) is consistently higher than the 2-meter vapor pressure (e_{2m}), with strong diurnal variability. The surface canopy temperature (T_c) is higher than the 2-meter temperature (T_{2m}) during the day, with a peak difference around local noon. At night, the surface temperature becomes lower than the 2-meter temperature as a result of longwave emission from the surface. The deep soil temperature (T_d) does not exhibit a diurnal cycle as defined. The soil wetness, or degree of saturation, is less in the first two layers than in the deep layer since evaporation and evapotranspiration remove moisture only from the first two layers. Only the soil moisture in surface layer exhibits a significant diurnal cycle.

Table 1 summarizes the four experiments, the two basic states, the leaf area index and the soil physical parameters. There are clear differences between the two basic states: the

temperature and surface vapor pressure values at 13Z for the June mean are higher than at 13Z June 1, and all three soil wetness values at 13Z for the June mean are consistently lower than those at 13Z June 1. The reason to use the same basic states for both grass and bare soil case is for comparisons, i.e., to see the effect of the different land-surface conditions. The vegetation and soil parameters also significantly differ between grass and bare soil. The "scaling values" in Table 1 are described in the next subsection.

Table 1: Experiment description. SW_i is soil wetness (the degree of saturation, $W_i/W_{i,sat}$), and $W_{i,sat}$ is the saturation moisture content in the ith soil layer. Z_i is the depth of a soil layer in meter. $\delta Z_{i,j}$ is the distance between the centers of ith and j^{th} soil layers. LAI is the leaf area index.

ITEM	EXP 1	EXP 2	EXP 3	EXP 4
Description of basic state and forcing terms	basic state and forcing terms from 13Z June 1 1986	basic state and forcing terms from 13Z for the June mean	basic state and forcing terms from 13Z June 1 1986	basic state and forcing terms from 13Z for the June mean
Vegetation type	grass	grass	bare soil	bare soil
Basic states:				
T_c (K)	18.27	26.08	18.27	26.08
T_d (K)	16.53	17.72	16.53	17.72
e_a (hPa)	18.95	22.64	18.95	22.64
SW_1	0.5439	0.4143	0.5439	0.4143
SW_2	0.5782	0.4948	0.5782	0.4948
SW_3	0.6910	0.6244	0.6910	0.6244
Parameters:				
LAI	3.671	3.671	0.001	0.001
$W_{1,sat}$ (mm)	8.4	8.4	4.0	4.0
$W_{2,sat}$ (mm)	197.4	197.4	4.0	4.0
$W_{3,sat}$ (mm)	420.0	420.0	130.56	130.56
Top layer Z_1	0.02	0.02	0.0092	0.0092
Middle layer Z_2	0.47	0.47	0.0092	0.0092
Bottom layer Z_3	1.00	1.00	0.30	0.30
$\delta Z_{1,2}$(m)	0.245	0.245	0.0092	0.0092
$\delta Z_{2,3}$(m)	0.735	0.735	0.1546	0.1546
Scaling Value:				
for T_c (K)	5.6	5.6	9.0	9.0
for T_d (K)	1.53	1.53	2.13	2.13
for e_a (hPa)	5.0	5.0	3.7	3.7
for W_1 (mm)	0.59	0.59	0.52	0.52
for W_2 (mm)	11.10	11.10	0.375	0.375
for W_3 (mm)	17.34	17.34	5.23	5.23

3.3 Tangent linear matrix calculation

The tangent linear matrices $A(\bar{X})$ for the four experiments were calculated using a centered difference scheme rather than an analytical derivative, as follows. For each experiment, six pairs of perturbed states $(\bar{X} + \delta x_j)$ and $(\bar{X} - \delta x_j)$, $j = 1, 2, ..., 6$, are formed. Here $\bar{X}$ is the basic state and δx_j is a perturbation, described below, around the jth component of the basic state. Six pairs of one-step integrations with the Mosaic LSM are then performed, to compute $\frac{F_i(\bar{X}+\delta x_j)-F_i(\bar{X}-\delta x_j)}{2\delta x_j}$ as an approximation to $A_{ij}(\bar{X})$ for $i, j = 1, 2, ..., 6$. Then the perturbation magnitude is reduced by a factor of two and the process is repeated. At the nth step, $\delta x_j = \frac{\delta x_j^{-1}}{2^{n-1}}$ for $j = 1, 2, ..., 6$, where δx_j^{-1} is the perturbation at the initial step. The process is halted when the successive matrices show sufficient convergence of their eigenvalues, as described in the following section. Thus we arrive at $A(\bar{X})$ for each of the four experiments.

The magnitudes of the initial perturbations should be meaningful, for example, larger than the size of measurement uncertainties in the land surface state. Also the perturbed states should stay within the local linear regime of the basic state. As shown for the control run, the basic state at noon satisfies the relationships $SW_3 > SW_2 > SW_1$, $T_c > T_{2m}$, and $e_a > e_{2m}$. The perturbed states should retain these relationships to stay within the linear regime. There are also numerous "conditionals" in the formulation of the Mosaic LSM. For example, soil moisture diffusion between two adjacent layers depends on the moisture gradient. If the perturbed state reverses this gradient, the soil moisture flux will abruptly change sign and magnitude. We carefully chose the perturbation magnitudes so that the perturbed states lie within the same regime as the basic state. The initial perturbation magnitude was $1\ ^0K$ for T_c and T_d, 1 hPa for e_a, 3% for the first and second layer soil wetness, and 5% for deep soil wetness.

An eigenanalysis is applied to each of the four matrices $A(\bar{X})$. The eigenvectors are nondimensionalized to enable comparison of their elements, and are also normalized to unity by dividing by the largest magnitude of the respective eigenvector elements. For EXP 1 and EXP 2, we select the scaling magnitudes as the standard deviations of each state variable at 13Z over the month of June from the control run. For EXP 3 and EXP 4, we performed a second control run with bare soil to obtain scaling magnitudes, since the standard deviations differ from the control run with grass (see scaling values in Table 1). The standard deviations at 13Z of June from this second control run are selected as the scaling magnitudes for EXP 3 and EXP 4.

4 Eigenanalysis of the tangent linear matrix

4.1 Eigenanalysis for the two experiments with vegetation cover

Table 2 lists the e-folding times (negative reciprocals of the eigenvalues) for EXP 1 for 3 successively smaller perturbations, denoted by P_i, $i = 1, 2, 3$. All eigenvalues are negative and real, indicating a locally stable and non-oscillatory system. The e-folding times range from 5 minutes (mode 1) to more than three months (mode 6). The e-folding times of the first five modes from the second perturbation are almost identical to those from the third perturbation, indicating convergence. The last mode shows some oscillation due to the numerical difficulty of solving for the minimum eigenvalue of a matrix with a wide range of eigenvalues; the ratio of the largest to the smallest eigenvalue exceeds four orders of magnitude.

Table 2: The e-folding times for EXP 1. The tangent linear matrix $A(\bar{X})$ was derived using successively smaller perturbations, indicated by P_1, P_2, and P_3.

PERT.	MODE 1	MODE 2	MODE 3	MODE 4	MODE 5	MODE 6
P_1	5.06 min	19.71 min	1.04 hr	3.15 day	11.52 day	111.93 day
P_2	5.06 min	19.68 min	7.60 hr	3.30 day	11.52 day	118.72 day
P_3	5.07 min	19.67 min	7.62 hr	3.30 day	11.52 day	104.85 day

Figure 2 shows the six normalized eigenvectors (modes) for EXP 1, corresponding to P_3 in Table 2. Each panel corresponds to one mode and the bars denote the magnitude of the elements. Each element is associated with one of the six prognostic variables or state perturbations. Our discussion will be qualitative, focusing on the dominant variables for each mode. While a moderate change of the scaling values would affect the quantitative appearance of Fig. 2, it would not affect the qualitative features.

The first mode shows that a perturbation in the surface vapor pressure e_a alone will decay quickly, with a 5-minute e-folding time. The second mode indicates a positive coupling of T_c with e_a. For this mode, a high surface temperature provides more energy for surface evaporation, and increases the moisture-holding capacity of the surface air. The near-surface air moisture gradient then increases, which stimulates more evaporation from the ground. This mode has a 20-minute e-folding time. The third mode shows a relatively weak negative coupling between the soil moisture in the top two layers. The fourth and sixth modes depict the coupling between the soil moisture in the three layers. The soil moisture transfer in the three layers exhibits two distinctive time scales. The fourth mode, representing soil moisture transfer from the third layer to the upper two layers (or the reverse), has about a 3-day e-folding time. The sixth mode, representing moisture transfer throughout the entire soil column, has a time scale of about 3 months. The fifth mode primarily isolates T_d with a 12-day e-folding time.

Table 3 lists the e-folding times for each mode of EXP 2. Again all eigenvalues are negative and real. The six eigenvectors corresponding to P_5 (Fig. 3) are similar to those of EXP 1. The e-folding times for most modes of EXP 2 are comparable to those of EXP 1. However, the third and sixth modes, which represent soil moisture transfer from the top soil layer and throughout the whole soil column, respectively, have much shorter time scales. The reduction in time scales of these two modes corresponds to the lower basic state soil wetness and the basic state of higher surface temperature and vapor pressure (Table 1) of EXP 2 compared with EXP 1.

Table 3: As in Table 2 but for EXP 2.

PERT.	MODE 1	MODE 2	MODE 3	MODE 4	MODE 5	MODE 6
P_1	5.03 min	16.21 min	4.49 hr	3.43 day	11.39 day	47.77 day
P_2	5.01 min	16.19 min	4.56 hr	3.56 day	11.41 day	51.65 day
P_3	5.01 min	16.86 min	4.61 hr	3.59 day	11.45 day	52.87 day
P_4	5.02 min	16.86 min	4.61 hr	3.59 day	11.45 day	48.92 day
P_5	5.00 min	16.88 min	4.61 hr	3.59 day	11.46 day	58.49 day

4.2 Eigenanalysis for the two experiments without vegetation cover

Table 4: As in Table 2 but for EXP 3.

PERT.	MODE 1	MODE 2	MODE 3	MODE 4	MODE 5	MODE 6
P_1	4.47 min	4.96 min	28.08 min	57.08 min	11.87 day	23.46 day
P_2	4.15 min	4.96 min	28.04 min	59.25 min	11.87 day	24.49 day
P_3	3.91 min	4.96 min	28.03 min	1.00 hr	11.87 day	24.57 day
P_4	3.73 min	4.96 min	28.03 min	1.03 hr	11.87 day	26.07 day
P_5	3.55 min	4.96 min	28.03 min	1.08 hr	11.82 day	21.47 day
P_6	3.55 min	4.96 min	28.03 min	1.08 hr	11.87 day	30.04 day

Table 4 and Fig. 4 show the eigenvalues and eigenvectors for EXP 3, which has the same basic state as EXP 1 but the surface is bare soil. The e-folding times of EXP 3, except for mode 5, are significantly shorter than those of both EXP 1 and EXP 2. The first three modes have time scales on the order of minutes. There are no intermediate modes with e-folding times between one hour and 10 days. The longest time scale is reduced to about a month.

Unlike EXP 1 and EXP 2, the first eigenvector of EXP 3 (Figure 4) represents soil moisture transfer between the first two adjacent soil layers. The e-folding time of this mode is about 4 minutes, which is much shorter than that of the corresponding (third) mode in EXP 1 and EXP 2. This reduction in time scale results from two factors. First, bare soil has no transpiration, so soil moisture evaporates directly from the surface. Second, the depth of the first two soil layers is shallow (see Table 1), so moisture transfer is fast. The second mode isolates e_a with a 5-minute time scale, which is similar to the first mode of the two previous experiments. The third mode shows the positive coupling between T_c and e_a with a 28-minute e-folding time, which is relatively long compared with the corresponding (second) mode in EXP 1 and EXP 2. Once again, the fourth and sixth modes depict two different soil moisture transfer processes, but now with shorter time scales. The fourth mode, with a one-hour time scale, shows a negative relationship between the soil moisture in the upper two layers and that of the third layer. The sixth mode, with about a one-month time scale, depicts transfer of moisture throughout the entire soil column. The fifth mode that primarily isolated T_d in EXP 1 and EXP 2 now also includes components of moisture. Its e-folding time is comparable to that in EXP 1 and EXP 2.

Table 5 lists the e-folding times for EXP 4. They are comparable with those of EXP 3, except that of mode 5 (around 3.5 days), which now represents soil moisture transfer throughout the entire soil column (compare with mode 6 of EXP 3, around 30 days). Figure 5 displays the eigenvectors for EXP 4. Similarly to EXP 3, the first eigenvector depicts a negative coupling between the soil moisture in the first two soil layers. However, e_a appears as a dominant variable in this mode. The second mode again isolates e_a. The third mode shows once more the coupling between T_c and e_a. Modes 4 and 5 represent significant moisture transfer among the model layers. Again, there is a mode isolating T_d, similar to mode 5 of EXP 3.

4.3 Summary of the four experiments

The results from all four experiments show common features even though different basic states and land covers were used. Tables 6 and 7 summarize the modes and associated

Table 5: As in Table 2 but for EXP 4.

PERT.	MODE 1	MODE 2	MODE 3	MODE 4	MODE 5	MODE 6
P_1	4.13 min	5.25 min	25.24 min	1.45 hr	3.15 day	13.03 day
P_2	4.30 min	5.25 min	25.19 min	1.46 hr	3.41 day	13.06 day
P_3	4.34 min	5.25 min	25.19 min	1.46 hr	3.50 day	13.07 day
P_4	4.35 min	5.25 min	25.18 min	1.46 hr	3.50 day	13.06 day
P_5	4.35 min	5.25 min	25.18 min	1.46 hr	3.48 day	13.05 day
P_6	4.35 min	5.25 min	25.18 min	1.46 hr	3.60 day	13.12 day
P_7	4.35 min	5.24 min	25.20 min	1.46 hr	3.56 day	13.06 day

physical processes. The e-folding times range widely in each experiment, indicating quite different characteristic time scales for different land surface processes. There are several distinct modes, including those isolating e_a, T_d, soil moisture transfer and coupling between T_c and e_a.

The two different basic states generally do not produce large differences in the eigenvalues (EXP 1 versus EXP 2, EXP 3 versus EXP 4). However, the mode that represents soil moisture transfer throughout the entire soil column shows a much shorter time scale when the basic state of 13Z for the June mean is used. This suggests that higher surface temperature and vapor pressure and lower soil wetness causes a soil moisture perturbation throughout the soil column to decay more quickly.

The eigenvectors of EXP 1 and EXP 2 are also similar, as are those of EXP 3 and EXP 4. However, the eigenvectors change significantly across the two groups. Note that the modes of soil moisture tend to be weakly coupled with other land surface state variables. This property will be further addressed in the next section.

It is hard to isolate the impact of vegetation in these experiments since the soil layer structure is significantly different between grass and bare soil. But the role of soil structure is clear. In the bare soil case (EXP 3, EXP 4), the three modes representing soil moisture transfer have much shorter e-folding times compared with those with the grass cover (EXP 1, EXP 2). Since the first two soil layers are shallow for the bare soil case, there is a negative coupling between these two soil moisture perturbations, as can be seen in the first panels of Figures 4 and 5.

The mode isolating the T_d perturbation has a consistent e-folding time across the four experiments. This is explained by examining the linearized T_d prognostic equation (2). The solution of the linearized equation shows that the e-folding time of a T_d perturbation is determined mainly by the soil heat capacity and the depth of the soil layer where the temperature varies slowly and does not have significant diurnal variability. In the Mosaic LSM, these parameters are the same for grass and bare soil.

11

Table 6: Description of the eigenmodes derived from EXP 1 and EXP 2. The e-folding times for EXP 2 are given in parentheses.

Mode Description	Mode #	e-folding Time
Dominant e_a perturbation.	Mode 1	5.07 (5.00) min
Coupling between T_c and e_a perturbations.	Mode 2	19.67 (16.88) min
Dominant W_1 perturbation.	Mode 3	7.62 (4.61) hr
Coupling of soil moisture in the three soil layers. Moisture perturbation in the deep layer has the opposite sign of that in the upper two layers.	Mode 4	3.30 (3.59) day
Dominant T_d perturbation.	Mode 5	11.52 (11.46) day
Coupling of soil moisture. Signs of the soil moisture perturbations are the same in the three layers.	Mode 6	104.85 (58.49) day

Table 7: Description of the eigenmodes derived from EXP 3 and EXP 4. The e-folding times and the different mode numbers for EXP 4 are given in parentheses.

Mode Description	Mode #	e-folding Time
Coupling of soil moisture between the upper two soil layers. In EXP 4, this coupling is associated with an e_a perturbation.	Mode 1	3.55 (4.35) min
Dominant e_a perturbation.	Mode 2	4.96 (5.24) min
Coupling between T_c and e_a perturbations.	Mode 3	28.03 (25.20) min
Coupling of soil moisture in the three soil layers. Moisture perturbation in the deep layer has the opposite sign of that in the upper two layers.	Mode 4	1.08 (1.46) hr
Dominant T_d perturbation.	Mode 5 (6)	11.87 (13.06) day
Coupling of soil moisture. Signs of the soil moisture perturbations are the same in the three layers.	Mode 6 (5)	30.04 (3.56) day

5 Eigenanalysis of the soil moisture dynamics subsystem

As we have seen, the modes representing the coupled evolution of soil moisture perturbations in all three layers have relatively long time scales, especially when there is a vegetation covering. This is important because it indicates that initial soil moisture errors will persist for a long time during nonlinear model integrations. Since these modes are only weakly coupled with other land-surface state variables in most cases, as suggested by the eigenvector patterns shown in Figs. 2-5, We therefore further examine the soil moisture dynamics using a 3 x 3 soil moisture dynamics subsystem.

The soil moisture dynamics subsystem consists of equations (4), (5), and (6). For convenience, we simplify these three equations by assuming the following: (1) the dependence of the surface runoff rate R_s on soil moisture is negligible, and (2) the soil wetness is moderate, therefore the relative humidity factor for the resistance to bare soil evaporation can be approximated as one.

Following the same procedure as in Section 3a, let $W_i = \bar{W}_i + W_i'$, we obtain the tangent linear model for the soil-moisture dynamics subsystem:

$$\frac{dW'}{dt} = BW' = (b_{i,j})\,W'. \tag{15}$$

Here W' is a vector consisting of the three soil moisture state perturbations, and B is the 3x3 Jacobian matrix of this soil moisture subsystem. By definition, B is a submatrix of the 6x6 Jacobian matrix A, with the two simplifications mentioned above. We obtain B analytically (the details of the derivation are not given in this paper). Again we evaluate this matrix with the basic states and land covering conditions described in Section 3b. The eigenvalues are solved numerically. The scaling magnitudes for the eigenvectors are also the same as those described in Section 3c.

We further examine the cubic equation for the eigenvalues. By applying several approximations we are able to derive simple, accurate, and explicit expressions that relate the key parameters of the system to the eigenvalues and the e-folding times.

5.1 Eigenvalues and eigenvectors

The tangent linear matrix for the soil moisture subsystem is nearly identical to the corresponding submatrix of the full system for each of the four experiments. The magnitudes of the elements generally differ from those of the full system by less than 1%. Again, all eigenvalues are negative and real. Table 8 lists the e-folding times of the subsystem for the four experiments. The modes of EXP 1 and EXP 2 again exhibit longer time scales than those of EXP 3 and EXP 4. The time scales are comparable with the corresponding ones derived from the 6-equation system (see Tables 6-7), except mode 1 for EXP 2 and mode 3 for EXP 4. These two modes in the six-equation system exhibit strong coupling between soil moisture and other state variables (see Figs. 3 and 5).

Figure 6 illustrates the three normalized eigenvectors for the soil moisture subsystem with the conditions of EXP 1. They agree quite closely with the corresponding modes of the full system (Fig. 2, modes 3, 4, and 6). Similarly, the normalized eigenvectors of the subsystem with the conditions of EXP 2, EXP 3, and EXP 4 exhibit close agreement with the corresponding modes of the full system shown in Figs. 3-5, even though some of these modes are strongly coupled with other state variables in the full system. This indicates that

Table 8: The e-folding times derived from the TLM of the soil moisture dynamics subsystem for the four experiments.

EXP. LABEL	MODE 1	MODE 2	MODE 3
EXP 1	7.46 hr	3.29 day	93.79 day
EXP 2	9.50 hr	3.89 day	75.57 day
EXP 3	3.57 min	1.09 hr	17.70 day
EXP 4	4.34 min	1.63 hr	12.37 day

the behavior of soil moisture perturbations in the full TLM can be approximated reasonably well by their behavior in the 3 x 3 TLM.

5.2 Key parameters

We now apply three successive simplifications to the 3 x 3 soil moisture dynamics subsystem that lead to explicit expressions for the dependence of the e-folding time scales on the key parameters. The e-folding time scales listed in Table 8 provide a baseline for comparison with the results of the approximations.

Approximation 1

We write the tangent linear matrix B as

$$\mathbf{B} = \begin{pmatrix} a & c & 0 \\ b & d & f \\ 0 & e & g \end{pmatrix},$$

where a, d, and $g < 0$, and b, c, e, $f > 0$ when B is evaluated with the basic state values $\bar{X}$ described in Section 3. The characteristic equation for the eigenvalues λ is:

$$\lambda^3 - (a + d + g)\lambda^2 + (ad + ag + dg - bc - ef)\lambda - (adg - aef - bcg) = 0. \quad (16)$$

Equation (16) is an expanded form of

$$(\lambda - \lambda_1)(\lambda - \lambda_2)(\lambda - \lambda_3) = 0$$

and the coefficients of the equation (16) are determined by the roots $\lambda_j (j = 1, 2, 3)$. For example, $a + d + g$ is the sum of three roots, $\lambda_1 + \lambda_2 + \lambda_3$.

Table 8 shows that three eigenvalues are separated from one another by an order of magnitude or more for each experiment. We adjust the approximation based on the clear separation of the three time scales. We write (16) as

$$\lambda^3 - C_2\lambda^2 + C_1\lambda - C_0 = 0. \quad (17)$$

The roots λ_j can be approximated, from the largest to the smallest, by:

$$\lambda_1 \cong \hat{\lambda}_1 \equiv C_2 = a + d + g, \quad (18)$$

$$\lambda_2 \cong \hat{\lambda}_2 \equiv \frac{C_1}{C_2} = \frac{ad + ag + dg - bc - ef}{a + d + g}, \tag{19}$$

$$\lambda_3 \cong \hat{\lambda}_3 \equiv \frac{C_0}{C_1} = \frac{adg - aef - bcg}{ad + ag + dg - bc - ef}. \tag{20}$$

The corresponding approximate e-folding times $\frac{-1}{\lambda_i}$ are given in Table 9. They agree well with those in Table 8.

Table 9: The approximate e-folding times derived from equations (18) to (20).

EXP. LABEL	MODE 1	MODE 2	MODE 3
EXP 1	6.79 hr	3.47 day	97.38 day
EXP 2	8.57 hr	4.08 day	79.88 day
EXP 3	3.38 min	1.14 hr	17.22 day
EXP 4	4.15 min	1.69 hr	11.69 day

Approximation 2

Further simplification is applied to equations (18) to (20) by neglecting small terms. Since the matrix B for EXP 1 (EXP 3) is very close to that for EXP 2 (EXP 4), only EXP 1 and EXP 3 are discussed here.

For EXP 1, a and b have the same magnitude but opposite signs, and the other elements are one order of magnitude smaller than a and b. Furthermore, $a + b$ is an order of magnitude smaller than a or b, and $c + d + e$ is three orders of magnitude smaller than c, d, or e. Therefore in the case of EXP 1 the approximate eigenvalues $\hat{\lambda}_i$ defined in Equations (18)-(20) are further approximated by $\tilde{\lambda}_i$, defined as follows:

$$\hat{\lambda}_1 \cong \tilde{\lambda}_1 \equiv a, \tag{21}$$

$$\hat{\lambda}_2 \cong \frac{ad + ag - bc}{a} \cong d + g + c \equiv \tilde{\lambda}_2, \tag{22}$$

$$\hat{\lambda}_3 \cong \frac{g(d + c) - ef}{d + g + c} \cong \frac{e}{e - g}(f + g) \cong \frac{2}{3}(f + g) \equiv \tilde{\lambda}_3, \tag{23}$$

where we have used the approximate relation $g \cong -0.5e$. The corresponding approximate e-folding times $\frac{-1}{\lambda_i}$ are 7.80 hours, 3.15 days, and 128 days, respectively, in good agreement with those shown in Table 8.

For EXP 3, the magnitudes of a, b, c, d, and e are similar, whereas f and g are about two orders of magnitude smaller. Again $|a + b| << |a|$ and $|c + d + e| << |c|$. Therefore we get:

$$\hat{\lambda}_1 \cong \tilde{\lambda}_1 \equiv a + d, \tag{24}$$

$$\hat{\lambda}_2 \cong \frac{ad - bc}{a + d} \cong \frac{a}{a + d}(c + d) \cong -0.37e \equiv \tilde{\lambda}_2, \tag{25}$$

$$\hat{\lambda}_3 \cong g - \frac{aef}{ad - bc} \cong g - \frac{ef}{c + d} \cong f + g \equiv \tilde{\lambda}_3, \tag{26}$$

15

where we have used the approximate relation $d \cong 2.7a$. The corresponding approximate e-folding times $\frac{-1}{\lambda_i}$ are 3.40 minutes, 1.28 hours, and 26.0 days, respectively. Again these values are close to those shown in Table 8.

Approximation 3

To get explicit relationships between the parameters or parameterizations and the e-folding times we further simplify the formulae above by including only the dominant terms in each element of matrix B. Tables 10 and 11 list the dominant terms for EXP 1 and EXP 3, respectively. The dominant terms for EXP 2 (EXP 4) are similar to those of EXP 1 (EXP 3). The notation shown in these tables is listed below:

K_i, ψ_i: soil hydraulic conductivity, and soil moisture potential in the ith layer

β: soil parameter related to the soil pore size distribution index

$\delta Z_{i,j}$: mean depth between the ith and j^{th} soil layers

For both grass and bare soil land conditions, the terms representing the impact of soil moisture fluxes on the evolution of soil moisture perturbations are important. The influence of evaporation and evapotranspiration does not stand out as a significant factor, because the selected basic state soil moisture values are not dry.

Table 10: $\hat{b}_{i,j}$, dominant terms of the tangent linear matrix of the soil moisture dynamics system, equation (15), with a grass land cover condition (EXP 1).

$\frac{dW'_i}{dt}$	$\hat{b}_{i,1}$	$\hat{b}_{i,2}$	$\hat{b}_{i,3}$
i=1	$\frac{\rho_w K_2 \beta \psi_1}{\delta Z_{1,2} W_1}$	$-\frac{\rho_w K_2 \beta \psi_2}{\delta Z_{1,2} W_2}$	0
i=2	$-\frac{\rho_w K_2 \beta \psi_1}{\delta Z_{1,2} W_1}$	$\frac{\rho_w K_2 \beta \psi_2}{\delta Z_{1,2} W_2} + \frac{\rho_w K_3 \beta \psi_2}{\delta Z_{2,3} W_2}$	$-\frac{2\beta+3}{W_3} Q_{2,3} - \frac{\rho_w K_3 \beta \psi_3}{\delta Z_{2,3} W_3}$
i=3	0	$-\frac{\rho_w K_3 \beta \psi_2}{\delta Z_{2,3} W_2}$	$\frac{2\beta+3}{W_3} Q_{2,3} + \frac{\rho_w K_3 \beta \psi_3}{\delta Z_{2,3} W_3} - \frac{2\beta+3}{W_3} Q_{3,\infty}$

Table 11: $\hat{b}_{i,j}$, dominant terms of the tangent linear matrix of the soil moisture dynamics system, equation (15), with a bare soil land cover condition (EXP 3).

$\frac{dW'_i}{dt}$	$\hat{b}_{i,1}$	$\hat{b}_{i,2}$	$\hat{b}_{i,3}$
i=1	$\frac{\rho_w K_2 \beta \psi_1}{\delta Z_{1,2} W_1}$	$-\frac{2\beta+3}{W_2} Q_{1,2} - \frac{\rho_w K_2 \beta \psi_2}{\delta Z_{1,2} W_2}$	0
i=2	$-\frac{\rho_w K_2 \beta \psi_1}{\delta Z_{1,2} W_1}$	$\frac{2\beta+3}{W_2} Q_{1,2} + \frac{\rho_w K_2 \beta \psi_2}{\delta Z_{1,2} W_2} + \frac{\rho_w K_3 \beta \psi_2}{\delta Z_{2,3} W_2}$	$-\frac{2\beta+3}{W_3} Q_{2,3} - \frac{\rho_w K_3 \beta \psi_3}{\delta Z_{2,3} W_3}$
i=3	0	$-\frac{\rho_w K_3 \beta \psi_2}{\delta Z_{2,3} W_2}$	$\frac{2\beta+3}{W_3} Q_{2,3} + \frac{\rho_w K_3 \beta \psi_3}{\delta Z_{2,3} W_3} - \frac{2\beta+3}{W_3} Q_{3,\infty}$

For EXP 1, the resulting expressions are:

$$\lambda_1 \cong \frac{\rho_w K_2 \beta \psi_1}{\delta Z_{1,2} \bar{W}_1},$$

$$\lambda_2 \cong \hat{b}_{3,3} + \frac{\rho_w K_3 \beta \psi_2}{\delta Z_{2,3} \bar{W}_2},$$

$$\lambda_3 \cong \frac{-2(2\beta + 3)Q_{3,\infty}}{3\bar{W}_3}.$$

The two of the corresponding e-folding times are 8.31 hr and 3.16 days, in good agreement with those of Table 8.

The first expression shows that the e-folding time $\frac{-1}{\lambda_1}$ is proportional to the mean depth $\delta Z_{1,2}$ and basic state soil moisture $\bar{W}_1$, and inversely proportional to the soil hydraulic conductivity K_2, soil moisture potential ψ_1, and soil constant b. Similarly, the e-folding time of the second mode increases with $\delta Z_{2,3}$, $\bar{W}_2$ and $\bar{W}_3$. It decreases with soil hydraulic conductivity K_3 and soil moisture potentials ψ_2 and ψ_3. The third e-folding time increases with the basic state soil moisture $\bar{W}_3$, and decreases when the moisture flux $Q_{3,\infty}$ through the bottom increases. Note that the soil moisture potentials are negative, and that the soil moisture fluxes $Q_{1,2}$ and $Q_{2,3}$ are negative with the selected soil moisture basic state, $\bar{W}_3 > \bar{W}_2 > \bar{W}_1$.

For EXP 3, by substituting the dominant terms, we get:

$$\lambda_1 \cong \hat{b}_{1,1} + \hat{b}_{2,2},$$

$$\lambda_2 \cong \frac{0.37\rho_w K_3 \beta \psi_2}{\delta Z_{2,3}\bar{W}_2},$$

$$\lambda_3 \cong \frac{-(2\beta + 3)Q_{3,\infty}}{\bar{W}_3}.$$

The three corresponding e-folding times are 3.40 min., 0.70 hours, and 26.5 days, respectively, with same magnitude scale as those of Table 8.

The relationships discussed for EXP 1 hold similarly for EXP 3. Table 12 summarizes these relationships between the e-folding times and the key parameters as well as the basic state. Of the key parameters, the mean depth between adjacent soil layers, $\delta Z_{1,2}$ and $\delta Z_{2,3}$, mainly accounts for the large differences in the e-folding times between the experiments with vegetation and without vegetation; the other key parameters are the same for grass and bare soil conditions in the Mosaic LSM.

Table 12: General relationships between the e-folding times and key parameters of the soil moisture subsystem.

Magnitude of e-folding time decreases with:	soil hydraulic conductivity: K_2, K_3 soil hydraulic potential: ψ_1, ψ_2, ψ_3 soil constant: β
Magnitude of e-folding time increases with:	basic state soil moisture: $\bar{W}_1$, $\bar{W}_2$, $\bar{W}_3$ mean depth between soil layers: $\delta Z_{1,2}$, $\delta Z_{2,3}$

6 Conclusions

This study explores a tangent linear analysis to a land surface model using a reasonable basic state and a simple land surface condition at the HAPEX site in summer-time. Several simplifications are made in the derivation of the TLM, including the assumption of a constant tangent linear matrix and the exclusion of interception storage. The eigenanalysis of TLM readily yields the characteristic time scales and the structure of the perturbed states of the Mosaic LSM. It effectively synthesizes the impact of different basic state and vegetation conditions on the linear evolution of initial errors. It also quantifies the intrinsic variability of the Mosaic LSM. An understanding of these features is important for developing a land-surface data assimilation scheme and for improving the physical parameterizations of an LSM.

The main results are summarized as follows:

(1) The Mosaic LSM exhibits a wide range of internal variability. The e-folding times of the different modes range from a few minutes to several months. Modes representing the evolution of perturbations in surface temperature and surface moisture exhibit short time scales. The modes representing the evolution of deep soil temperature perturbations and soil moisture perturbations coupled within the whole soil column exhibit longer time scales. The mode representing the deep soil temperature (T_d) perturbation is weakly coupled to the other land-surface variables and has a consistent e-folding time across the experiments.

(2) The e-folding time scales depend clearly upon soil layer depth, soil parameters, and basic state conditions. In particular, the modes representing the behavior of soil moisture perturbations have significantly longer time scales for the deep soil layer. The influence of the difference in basic states studied here is small because they are rather similar to each other. However, warmer surface temperature and higher surface-air moisture tend to shorten the e-folding times.

(3) For the simplified soil moisture dynamics subsystem, the terms representing soil moisture fluxes are the most important factors for determining the time scales. The effect of evaporation and evapotranspiration is much less significant, simply because we have chosen a fairly moist basic state soil moisture. The key parameters determining the e-folding time scales include the mean depth between soil layers, the soil hydraulic conductivity and potential, the soil parameter β, and the basic state soil moisture. Deeper and wetter soils have longer time scales, and larger soil parameter β and higher soil hydraulic conductivity and potential tend to shorten time scales.

(4) The Mosaic LSM is stable for the basic states used. Any initial perturbation, or initial error, will decay with time. The formulation of the Mosaic LSM appears to prevent instabilities.

The results qualitatively agree with previous studies. In particular, the importance of accurate soil moisture and the longer time scale of soil moisture have been pointed by previous studies (i.e., Robock et al. 1998; Schlosser et al., 1997; Vinnikov et al. 1996; Yang et al. 1995; Yang et al., 1994). For example, Robock et al. (1998) gave a comprehensive evaluation of soil moisture simulated by the models of Atmospheric Model Intercomparison Project (AMIP) based on soil moisture observations. They pointed out a long-term (1-4 months) scale in soil moisture variation and that the key parameter of soil field capacity is the maximum soil moisture held in a column. Soil layer structure is related to this parameter. Our study provides a new perspective to view these time scales and key parameters.

We must be careful when generalizing the results of this study. First, the results were obtained with respect to two types of land conditions, and the basic state was held constant in time when deriving the TLM. For different atmospheric and vegetation conditions, eigen-

values and eigenvectors will be different. The methodology employed here does not apply directly to an actual time-varying basic state. Second, the tangent linear approach itself applies, in principle, to small perturbations only. The linear approximation does not always hold. A thorough discussion regarding this issue is given by Errico (1997). Finally, the precise interpretation of the eigenmodes we have obtained depends on our choice of scaling magnitudes. These were derived empirically based on standard deviations from the control runs. They are perhaps comparable to measurement uncertainties, but would be different, for instance, for different land surface regimes.

Acknowledgments

References

Brubaker, K.L., and D. Entekhabi, An analytic approach to modeling land-atmosphere interaction 1. Construct and equilibrium behavior. *Water Resources Research, 3,* 619-632,1995.

Chen, T.H., A. Henderson-Sellers, P.C.D. Milly, A. J. Pitman, A.C.M Beljaars, and 38 others, Cabauw experimental results from the Project for Intercomparison of Land surface Parameterization Schemes (PILPS), *J. Climate, 10,* 1194-1215, 1997.

DAO, 1996: Algorithm Theoretical Basis Document Version 1.01, Data Assimilation Office, NASA Goddard Space Flight Center, Greenbelt, MD 20771. Available on the internet at
http://dao.gsfc.nasa.gov/subpages/atbd.html.

Delworth and Manabe, The influence of potential evaporation on the variabilities of simulated soil wetness and climate. *J. Climate, 1,* 523-547, 1988.

Delworth and Manabe, Climate variability and land-surface processes. *Advances in Water Resources, 16,* 3-20, 1993.

Dickinson, R.E., Modeling evapotranspiration for three-dimensional global climate models. In *Climate Processes and Climate Sensitivity.* **Geophysical Monograph, 29.** American Geophysical Union, Washington, D.C. 58-72, 1984.

Entekhabi, D., Recent advances in land-atmosphere interaction research. *Reviews of Geophysics.* Supplement. 995-1003, 1995.

Errico, R.M., What is an adjoint model? *Bull. Amer. Meteor. Soc., 78,* 2577-2590, 1997.

Goutorbe, J.P., A critical assessment of the SAMER network accuracy. *Land surface Evaporation.* Ed. Schmugge and Andre, Springer-Verlag, 171-182, 1991.

Goutorbe, J.P. and C. Tarrieu, HAPEX-MOBILHY data base. *Land surface Evaporation.* Ed. Schmugge and Andre, Springer-Verlag, 403-410,1991.

Henderson-Sellers, A., Z.-L. Yang, and R. E. Dickinson, The Project for Intercomparison of Land-surface Parameterization Schemes. *Bull. Am. Meteorol. Soc., 74,* 1335-1349, 1993.

Henderson-Sellers, A., B. Henderson-Sellers, D. Pollard, J. M. Verner, and A.J. Pitman, Applying software engineering metrics to land surface parameterization schemes. *J. Climate, 8,* 1043-1059, 1995.

Koster, R.D, and M.J. Suarez, Modeling the land surface boundary in climate models as a composite of independent vegetation stands. *J. Geophys. Res., 97,* 2697-2715, 1992.

Koster, R.D, and M.J. Suarez, The components of a SVAT scheme and their effects on a GCM's hydrological cycle. *Adv. Water Resour., 17,* 61-78, 1994.

Koster, R.D, and M.J. Suarez, Energy and Water Balance Calculations in the Mosaic LSM. *NASA Technical Memorandum 104606, 9,* 1996.

Liang, X., E.F. Wood, D. P. Lettenmaier, D. Lohmann, and 25 others, The project for the intercomparison of land-surface parameterization schemes (PILPS) phase 2(c) Red Arkansas river basin experiment, 2, Spatial and temporal analysis of energy fluxes. *J. Global and Planetary Change, 19,* 137-159, 1998.

Molod, A. The Land Surface Component in GEOS: Model Formulation. *DAO Office Note., 3,* 1999.

Robock, A., C.A. Schlosser, K.Y. Vinnikov, N.A. Speranskaya, J.K. Entin, and S. Qiu, Evaluation of AMPI soil moisture simulations. *Global and Planetary Change, 19*, 181-208, 1998.

Sato, N., P.J. Sellers, D.A. Randall, E.K. Schneider, J. Shukla, J.L. Kinter, III, Y.-T. Hou, and E. Albertazzi, Effects of implementing the simple biosphere model in a general circulation model. *J. Atmos. Sci., 46*, 2757-2782, 1989.

Schlosser, C., A. Robock, K. Ya. Vinnikov, N.A. Speranskaya, and Y. Xue, 18-year land surface hydrology model simulations for a midlatitude grassland catchment in Valdai, Russia. *Mon. Wea. Rev., 125*, 3279-3294, 1997.

Scott, R., D. Entekhabi, R. Koster, and M. Suarez, Time scales of land surface evapotranspiration response. *J. Climate, 10*, 559-566, 1997.

Sellers, P.J., Y. Mintz, Y.C. Sud, and A. Dalcher, A simple biosphere model (SiB) for use within general circulation models. *J. Atmos. Sci., 43*, 505-531, 1986.

Vinnikov, K. Y., A. Robock, N.A. Speranskaya, C.A. Schlosser, Scales of temporal and spatial variability of midlatitude soil moisture. *J. Geophys. Res., 101*, 7163-7174, 1996.

Wood, E.F., D. P. Lettenmaier, X. Liang, D. Lohmann, and 25 others, The project for the intercomparison of land-surface parameterization schemes (PILPS) phase 2(c) Red Arkansas river basin experiment, 1, Experiment description and summary intercomparisons, *J. Global and Planetary Change, 19*, 115-135, 1998.

Xue, Y., H.G. Bastable, P. A. Dirmeyer, and P.J. Sellers, Sensitivity of simulated surface fluxes to changes in land surface parameterization – a study using ABRACOS data. *J. Appl. Meteor., 35*, 386-400, 1996a.

Xue, Y., F. J. Zeng, and C.A. Schlosser, SSiB and its sensitivity to soil properties — a case study using HAPEX-Mobilhy data. *Global and Planetary Change, 13*, 183-194, 1996b.

Yang, R., J. Shukla, and P.J. Sellers, The influence of changes in vegetation type on the surface energy budget. *Advances in Atmospheric Sciences, 11*, 139-161, 1994.

Yang, Z.L., R. E. Dickinson, A. Henderson-Sellers, and A.J. Pitman, Preliminary study of spin-up processes in land surface models with the first stage data of Project for Inter-comparison of Land Surface Parameterization Scheme Phase 1a (PILPS). *J. Geophys. Res., 100*, 16553-16578, 1995.
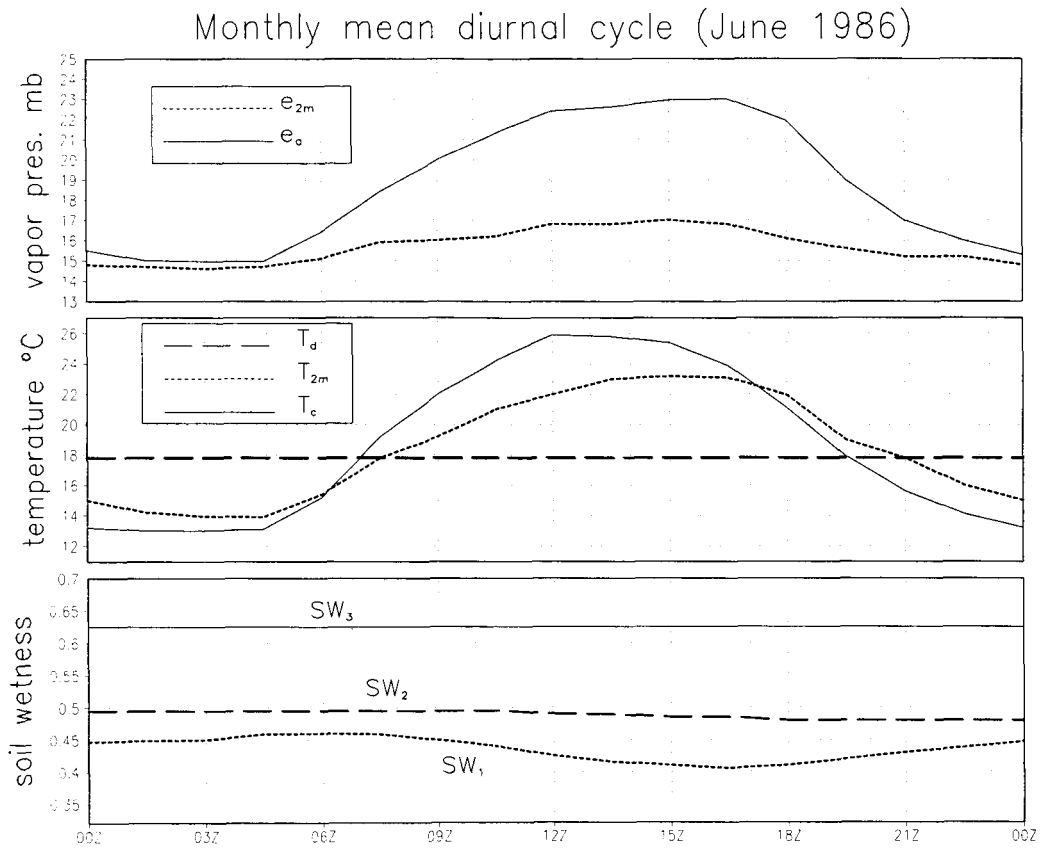
Monthly mean diurnal cycle (June 1986)

Figure 1: Monthly mean diurnal cycles averaged from the second June of a three-year Mosaic LSM integration forced by a time series of observed atmospheric conditions at the HAPEX-Mobilhy Caumont site. Upper panel: water vapor pressure in canopy air e_a (solid line) and 2-meter water vapor pressure e_{2m} (dashed line), in hPa. Middle panel: ground temperature T_c (solid line), deep soil temperature T_d (long-dashed line), and 2-meter air temperature T_{2m} (short-dashed line), in C^0. Bottom: soil wetness in the first layer SW_1 (short-dashed line), root layer SW_2 (long-dashed line), and the deep layer SW_3 (solid line).
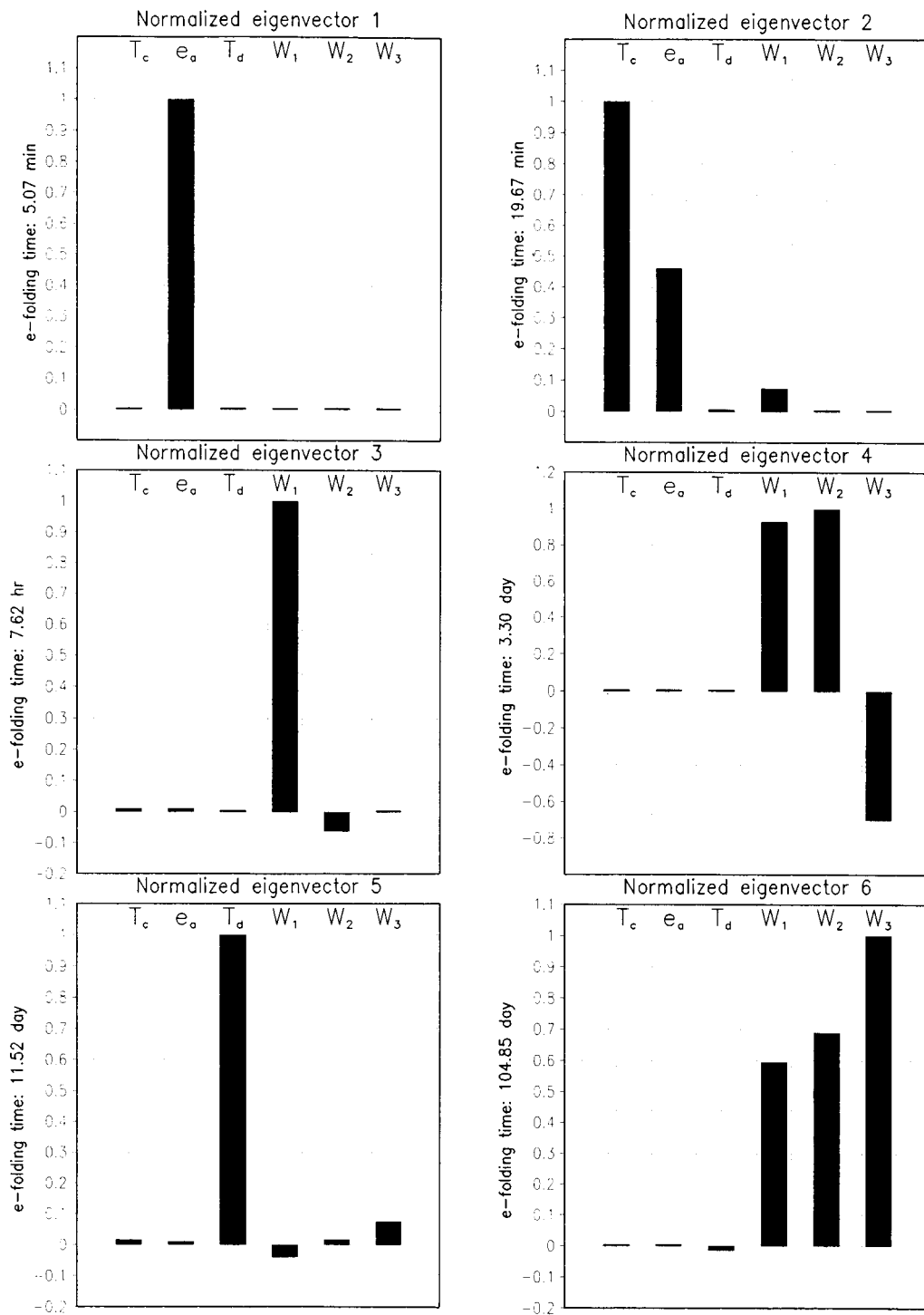
Figure 2: Six normalized eigenvectors, in order of increasing time scale, derived from the TLM for EXP 1. A bar denotes the magnitude of each variable.
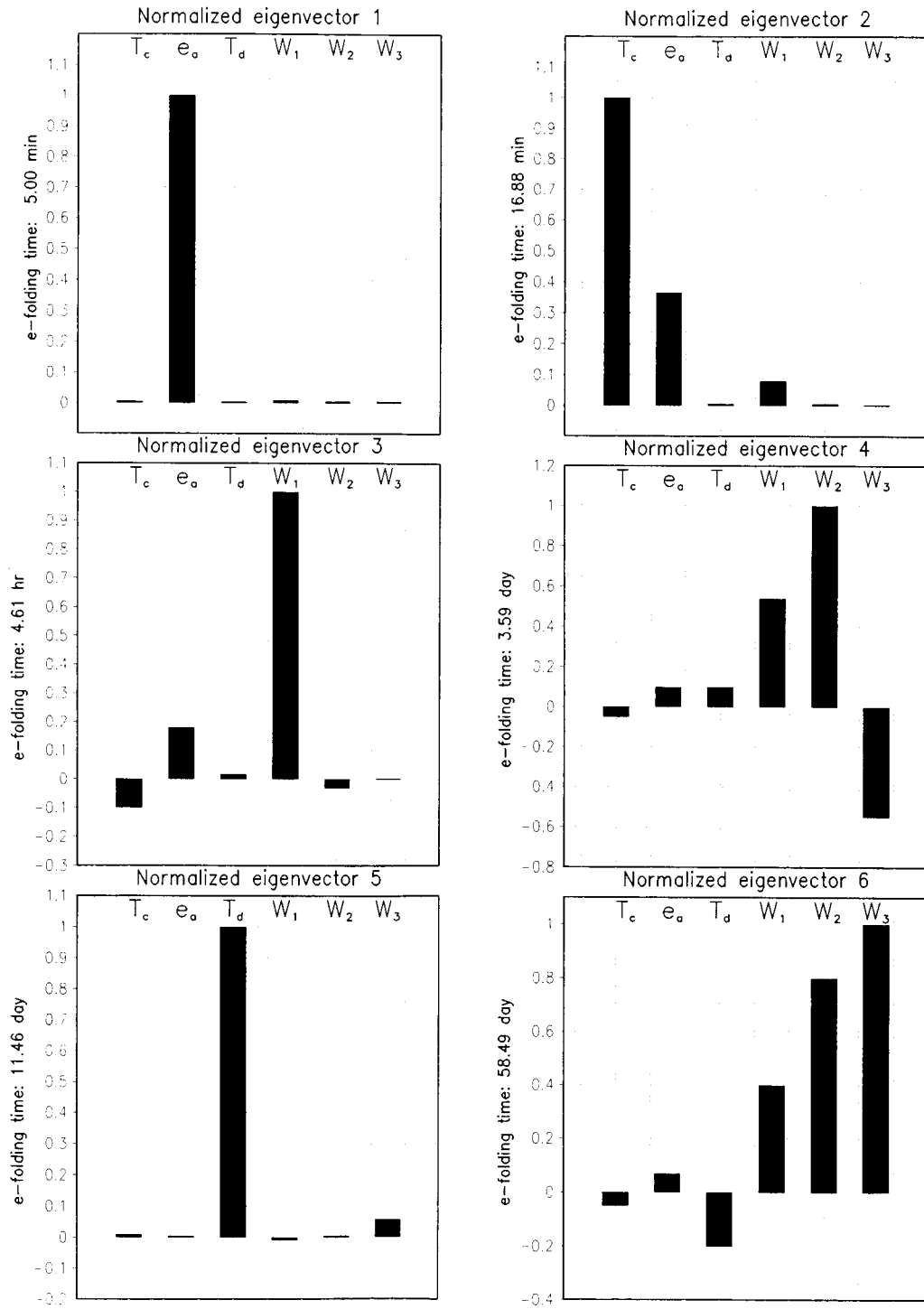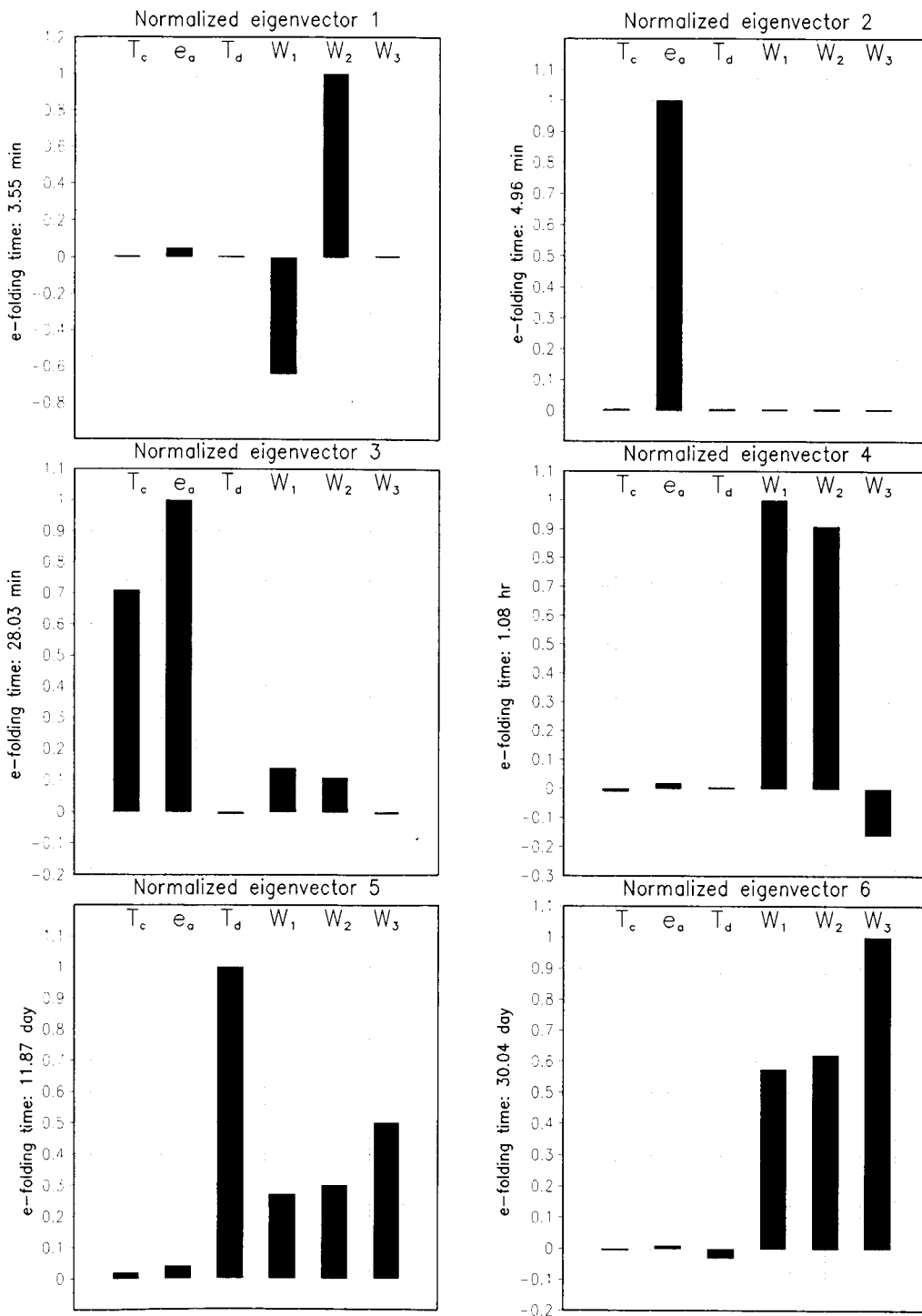
Figure 3: Same as Fig. 2 but for EXP 2.

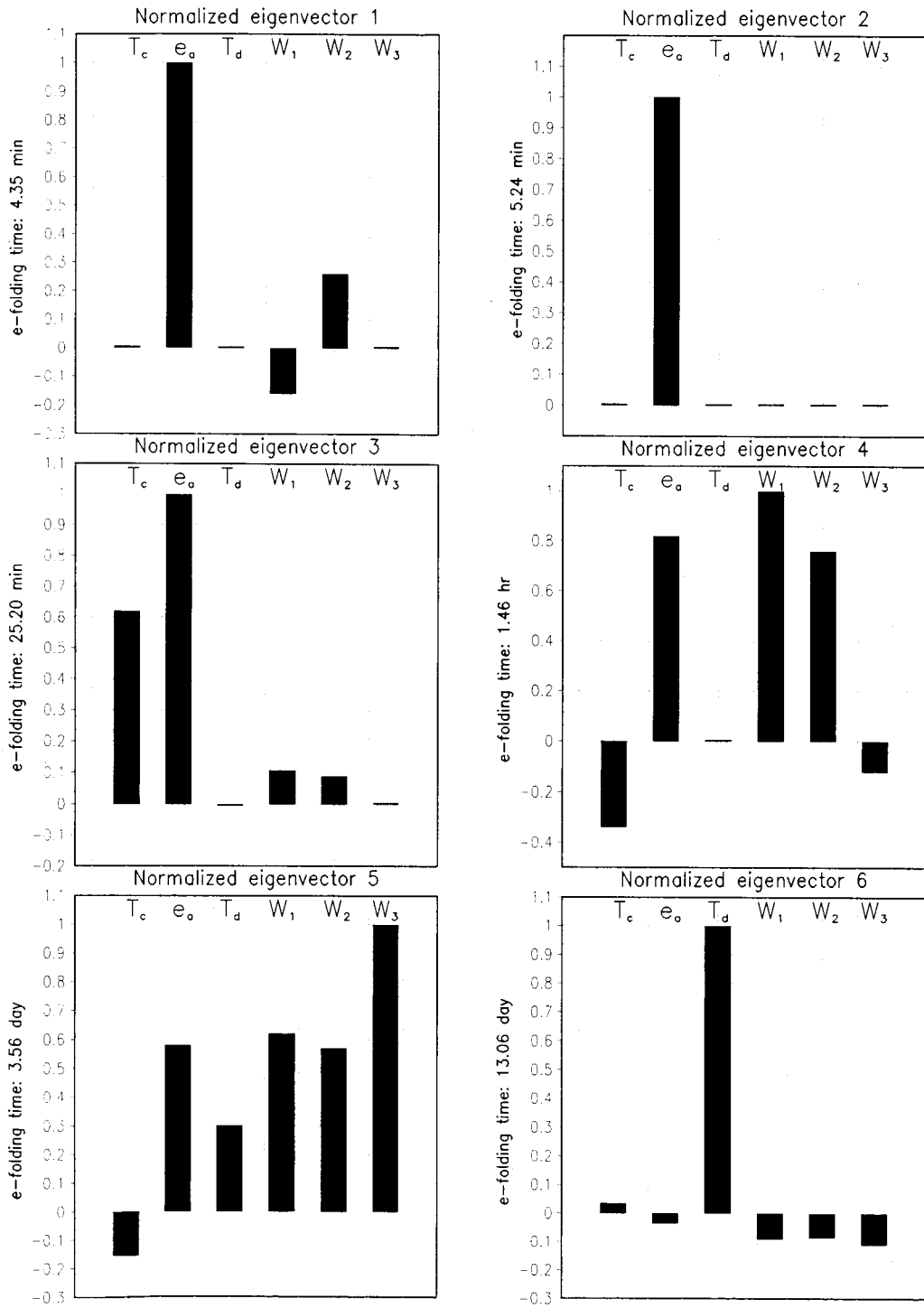24

Figure 4: Same as Fig. 2 but for EXP 3.
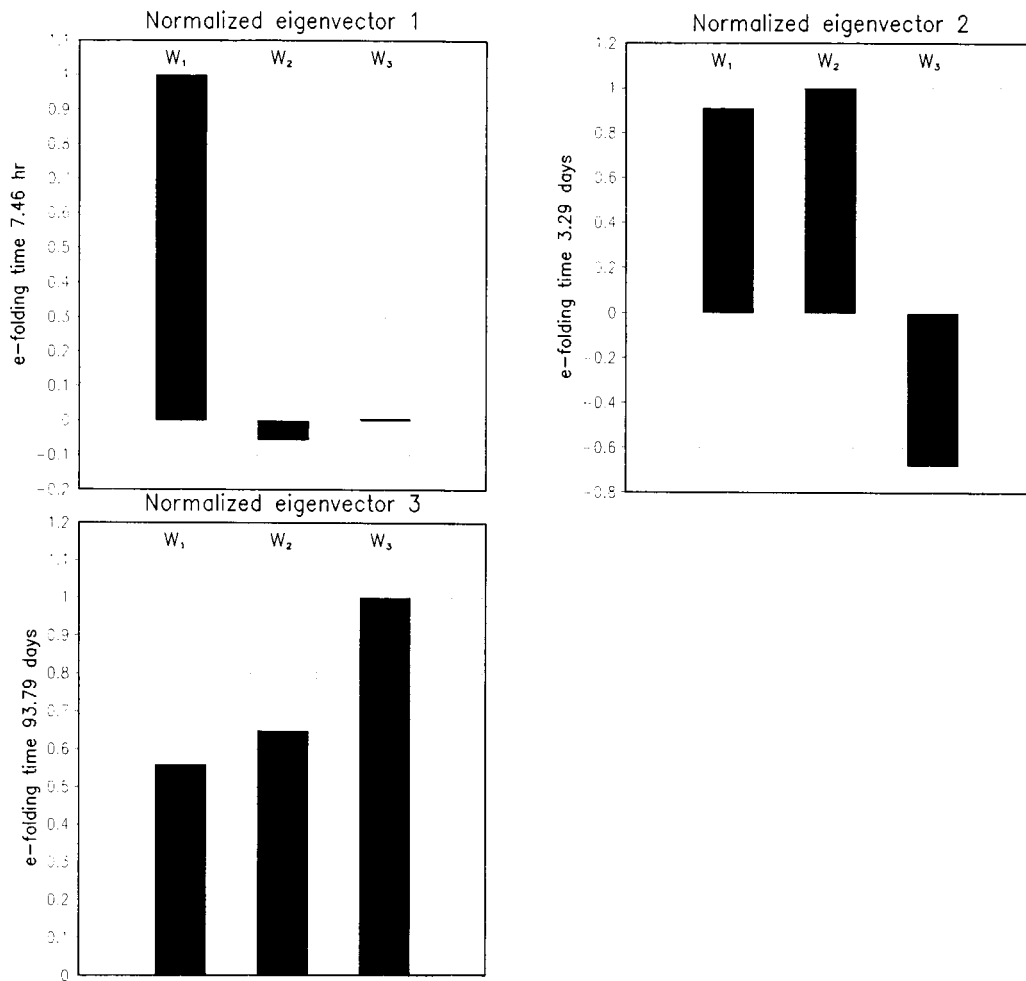
25

Figure 5: Same as Fig. 2 but for EXP 4.

Figure 6: Three normalized eigenvectors, in order of increasing time scale, derived from the soil moisture dynamics subsystem under the conditions of EXP 1.